



1 **Development of a sequential tool, LMDZ-NEMO-med-V1,**  
2 **to conduct global to regional past climate simulation for**  
3 **the Mediterranean basin: An Early Holocene case study**  
4

5 Tristan Vadsaria<sup>1</sup>, Laurent Li<sup>2</sup>, Gilles Ramstein<sup>1</sup> and Jean-Claude Dutay<sup>1</sup>

6 <sup>1</sup>Laboratoire des Sciences du Climats et de l'Environnement, CEA-CNRS- Université Paris Saclay, Gif-  
7 sur-Yvette, 91191, France

8 <sup>2</sup>Laboratoire de Météorologie Dynamique, CNRS-ENS-Ecole Polytechnique- Sorbonne Université,  
9 Paris, 75005, France

10 *Correspondence to:* Tristan Vadsaria (tristan.vadsaria@lsce.ipsl.fr)

11 **Abstract**

12 Recently, major progress has been made in the simulation of the ocean dynamics of the Mediterranean  
13 using atmospheric and oceanic models with high spatial resolution. High resolution is essential to  
14 accurately capture the synoptic variability required to initiate intermediate and deep-water formation,  
15 the engine of the MTC (Mediterranean Thermohaline Circulation). In paleoclimate studies, one major  
16 problem with the simulation of regional climate changes is that boundary conditions are not available  
17 from observations or data reconstruction to drive high-resolution regional models. One consistent way  
18 to advance paleoclimate modelling is to use a comprehensive global to regional approach. However, this  
19 approach needs long-term integration to reach equilibrium (hundreds of years), implying enormous  
20 computational resources. To tackle this issue, a sequential architecture of a global-regional modelling  
21 platform has been developed and is described in detail in this paper. First of all, the platform is validated  
22 for the historical period. It is then used to investigate the climate and in particular, the oceanic  
23 circulation, during the Early Holocene. This period was characterised by a large reorganisation of the  
24 MTC that strongly affected oxygen supply to the intermediate and deep waters, which ultimately led to  
25 an anoxic crisis (called sapropel). Beyond the case study shown here, this platform may be applied to a  
26 large number of paleoclimate contexts from the Quaternary to the Pliocene, as long as regional tectonics  
27 remain mostly unchanged. For example, the climate responses of the Mediterranean basin during the  
28 last interglacial (LIG), the last glacial maximum (LGM) and the Late Pliocene, all present interesting  
29 scientific challenges which may be addressed using this numerical platform.

30 **1 Framework of the study**

31 **1.1. Introduction**

32 The Mediterranean basin is a key region for the global climate system and is considered to be a climate  
33 “hotspot” (Giorgi, 2006), due to its high sensitivity to global warming. In the past, it has been the seat  
34 of important human civilisations, and it continues to play a very important role in international  
35 geopolitics with a dense population along its coasts. There is great diversity in the Mediterranean



36 ecosystems, both marine and terrestrial. The Mediterranean region is also rich in paleoclimate records  
37 with a variety of proxies. Indeed, this area experienced major changes during the glacial-interglacial  
38 cycles (Jost et al., 2005; Ludwig et al., 2018; Ramstein et al., 2007). Another long-term cycle of changes  
39 due to high-frequency precession which drastically modified the hydrological patterns of this area  
40 (monsoon, sapropels) is also superimposed.

41

42 Due to the peculiarities of both the atmospheric and oceanic circulation in the region, high-quality  
43 climate modelling of the Mediterranean region needs to have high spatial resolution. Indeed, the  
44 presence of strong gusts of wind in winter are essential to trigger oceanic convection and these can only  
45 be correctly represented in high-resolution models. Limited area models (LAM), or regional climate  
46 models (RCM), present some advantages in this regard, since they generally demand less computing  
47 resources, allowing them to be run at high spatial resolution for a given region. However, their  
48 usefulness for paleoclimate purposes is limited because of the lack of adequate lateral boundary  
49 conditions to drive the RCMs. The main reason why few comprehensive modelling exercises to explain  
50 paleoclimate changes around the Mediterranean have been performed is that the level of computing  
51 resources required for high resolution and long simulations is inaccessible. This is especially true in the  
52 case of the Mediterranean Thermohaline Circulation (MTC), which has significantly changed in the  
53 past, at both centennial and millennial scales.

54

55 In this paper, we developed a modelling suite to define high-resolution atmospheric conditions over the  
56 Mediterranean basin from global ESM (Earth System Model) paleoclimate simulations. In a second step,  
57 we used this atmospheric forcing to run a highly resolved ocean model (NEMOMED8 1/8°) to  
58 accurately simulate ocean dynamics. This tool allows us to achieve a high spatial resolution and  
59 equilibrated simulations with a run time of 100 years. The objective of this study is to develop a  
60 modelling platform sufficiently comprehensive to conduct paleoclimate studies of the Mediterranean  
61 basin. The potential of this platform is illustrated by investigating climate situations from the present  
62 period and from the Early Holocene that generated sapropel events.

63

64 The sapropel events provide excellent case studies on the impact of global changes on the Mediterranean  
65 basin. These periodic events are related to a long period of anoxia of the deep and bottom waters  
66 triggered by an enhancement of the African monsoon caused by periodicities of the orbital precession.  
67 However, the localisation of the forcing source caused by orbital variability is still a subject of debate.  
68 This is especially true for the last sapropel, denoted S1, which occurred during the early Holocene  
69 (between 10500 and 6800 ka BP) (De Lange et al., 2008). Reproducing past climate variations over the  
70 Mediterranean basin, including the sapropel events, is therefore a challenge for the modelling  
71 community.

72



73 The paper is organised as follows: In the first part, we briefly review the different approaches used to  
74 simulate the Mediterranean climate and sea conditions, and we present the concept of the sequential  
75 procedure that we propose. In a second part, we present in detail the model architecture we developed.  
76 Finally, we present applications with simulations of the historical period (1970-1999) and the Early  
77 Holocene (around 9.5 ka).

## 78 **1.2. Overview of current Mediterranean Sea modelling**

79 The Mediterranean Sea, due to its limited size and its semi-enclosed configuration, has a faster  
80 equilibrium response (100 year) than the global ocean (1000 year). Because of this semi-enclosed  
81 configuration, there are a few requirements that modelling of the Mediterranean Sea needs to satisfy so  
82 that its evolution can be properly represented. High resolution in both the atmospheric forcing and the  
83 oceanic configuration is necessary to correctly simulate the convection areas and the associated  
84 thermohaline circulation (Lebeaupin Brossier, et al., 2011). Depending on the mechanism studied, the  
85 resolution of the ocean model used by the research community ranges from  $1/4^\circ$  (e.g. for paleo-climatic  
86 simulation), to  $1/75^\circ$  (for hourly description of the mixed layer, tide-based investigation). The results  
87 for oceanic convection are highly dependent on the flux of heat and water and the wind stress at the air-  
88 sea interface, especially the seasonal variability and intensity. There are many modelling configurations  
89 in the scientific literature making it impossible to provide an exhaustive review of all of them. We can  
90 summarise them by presenting the different approaches used to drive the Mediterranean oceanic model,  
91 along with their advantages and drawbacks. We underline our new, coherent method, which captures  
92 the changes in ocean dynamics in the Mediterranean basin derived from global paleoclimate simulations.  
93

### 94 *Observations and reanalysis*

95 The most common way to simulate the general circulation of the Mediterranean Sea is to run a regional  
96 oceanic general circulation model forced by surface fluxes and wind stresses derived from observations  
97 and reanalyses. In this way, an oceanic model can be driven by realistic fluxes. In most cases, it implies  
98 a spatial atmospheric resolution of less than 50 km and a daily temporal resolution, at a minimum, in  
99 order to simulate the formation of dense water (Artale, 2002). This approach is adapted to simulate the  
100 present-day Mediterranean Sea and to explore the complexity of its sub-basin circulation and water mass  
101 formation (Millot and Taupier-Letage, 2005). However, this method is not well adapted to the study of  
102 past and future climate.

103

### 104 *Atmospheric model*

105 A second method consists of forcing a regional oceanic model with simulations from an atmospheric  
106 model, AGCM (Atmospheric Global Climate Model) or ARCM (Atmospheric Regional Climate  
107 Model). Since the AGCM resolution (typically 100 to 300 km horizontally) is coarse, statistical and/or



108 dynamical downscaling is usually needed, especially for wind-stress so that the ORCM (Ocean Regional  
109 Circulation Model) can be correctly forced (Béranger et al., 2010). Currently, dynamical downscaling  
110 with ARCM is the preferred option because it generally improves simulations of the climate in the  
111 Mediterranean region and especially of the hydrological cycle (Li et al., 2012).

112

113 This configuration is broadly used to assess anthropogenic climate changes (Adloff et al., 2015; Macias  
114 et al., 2015; Somot et al., 2006). In these studies, the Mediterranean Sea simulations are generally driven  
115 by the outputs of an ARCM, which is, in turn, driven by the GCM or observations. It should be noted  
116 that biases in oceanic variables can be reduced through constant flux correction (Somot et al., 2006).  
117 This configuration is suitable for high-resolution simulation of the past Mediterranean Sea  
118 (Mikolajewicz, 2011 for the LGM; Adloff et al., 2011 for the Early Holocene among others).

119

#### 120 *Regional coupled model*

121 Although the majority of the Mediterranean Sea models are ocean-alone models, some of them use a  
122 coupled configuration between the Mediterranean Sea and the atmosphere. Such a coupled configuration  
123 generally improves the simulation of the air-sea fluxes, including their annual cycle (de Zolt et al., 2003),  
124 but may show climate drifts in key parameters such as the SST. Regional coupled models are now  
125 emerging as a tool in Mediterranean climate modelling (Artale et al., 2010; Dell'Aquila et al., 2012;  
126 Drobinski et al., 2012; Sevault et al., 2014; Somot et al., 2008). However, this full-coupling  
127 configuration is currently not possible for high-resolution paleoclimate issues requiring long simulation.

128

#### 129 *Importance of boundary conditions*

130 The boundary conditions applied to the Mediterranean Sea domain, in particular, the exchanges of water,  
131 salt and heat with the Atlantic Ocean through the Strait of Gibraltar modulate significantly the  
132 Mediterranean circulation (Adloff et al., 2015). This is especially true at the millennial scale where  
133 deglaciation episodes and fluctuations of the AMOC (Atlantic Meridional Overturning Circulation) and  
134 the Mediterranean Sea affect each other (Swingedouw et al., 2018). The level of discharge from the  
135 main rivers is also crucial as is illustrated by the sapropel episodes, where an increase in freshwater  
136 input drastically slowed down the MTC. Most of current models impose prescribed (observed when  
137 possible) conditions in the near Atlantic zone, including temperature and salinity. The same  
138 methodology can be used to prescribe river discharges. However, it must be acknowledged that  
139 determining inputs from rivers into the Mediterranean Sea, either of water or other materials, still  
140 presents serious challenges for modelling.



### 141 **1.3. Concepts for a sequential procedure to perform global-to-regional modelling**

142 In this paper, we propose a new architecture for high-resolution modelling of the climate of the  
143 Mediterranean basin for past, present and future climates. This architecture is based on a method as  
144 much consistency between the models as possible and high congruency with data.

145

#### 146 *Step 1: Global climate*

147 Our goal is to simulate different climate conditions for the Mediterranean basin. The first step of any  
148 relevant procedure should be to simulate the global climate conditions from which we drive the  
149 simulation of the regional climate. These may be already available in simulations from previous PMIP  
150 exercises for various periods (e.g. mid-Holocene, Last Glacial Maximum, Last Interglacial and mid-  
151 Pliocene) as well as for different sapropel events and interglacials (e.g. MIS11, MIS13 and MIS19).  
152 However, this is not always possible due to the large volume of high-frequency 3-D atmospheric  
153 circulation variables involved. An alternative approach, used in some regional climate simulations  
154 (Chen et al, 2011; Goubanova & Li, 2007; Krinner et al, 2014), consists of using an AGCM (either an  
155 independent one or the same one used for the global climate simulation) run with appropriate values for  
156 global Sea Surface Temperature (SST) and Sea Ice cover (SIC). SST is crucial to determine atmospheric  
157 features and responses, while SIC plays a key role in determining the global albedo. Monthly SST and  
158 SIC are necessary and sufficient to drive an AGCM. They can be acquired from global climate  
159 simulations or through a bias-correction procedure.

160

#### 161 *Step 2: Regional climate*

162 After running an AGCM, regional climate can be now reproduced with an ARCM nested into the high-  
163 frequency outputs from the AGCM. Of course, the ARCM can be run in parallel to the AGCM, or with  
164 a small time delay. Thus, we avoid a large accumulation of intermediate information between the AGCM  
165 and the ARCM. In our study, we assume that there would be no feedback from the regional scale to the  
166 global scale, so only a “one-way” transfer of information (from global to regional) is considered. In our  
167 case, the ARCM is a strongly zoomed-in version of the AGCM and is also driven by monthly SST and  
168 SIC values. The higher resolution of the ARCM allows the synoptic variability and seasonality of the  
169 Mediterranean region to be depicted so that a realistic wind pattern and hydrological cycle may be  
170 reproduced. This approach provides a general framework for use in many different paleoclimate periods  
171 from the Pliocene to the Pleistocene, as long as the basin tectonics remain unchanged.

172

#### 173 *Step 3: Mediterranean Sea Circulation*

174 Daily air-sea fluxes and wind stress provided by the ARCM are used as surface boundary conditions to  
175 drive the ORCM to investigate the oceanic dynamics of the Mediterranean. It is reasonable to assume  
176 that the boundary conditions of these air-sea fluxes represent the long-term trends of the oceanic  
177 dynamics. Rivers may be considered interactive or not depending on the investigative objectives: runoff



178 can be prescribed from climatology or obtained from the hydrological component of the surface model.  
179 Again, we highlight that our architecture does not include any feedback, between either the regional  
180 ocean and the regional atmosphere, or the regional ocean and the global ocean. This configuration means  
181 that we can avoid dealing with certain issues, for example, the influence of the Mediterranean Outflow  
182 Water on the North Atlantic Ocean but is well adapted to provide consistent river runoff associated with  
183 changes in continental precipitation.

## 184 **2 Model architecture**

185 We used an ensemble of modelling tools that includes two atmospheric models and a regional oceanic  
186 model. Figure 1 summarises the configuration and shows the experimental flowchart.

### 187 **2.1. The atmospheric models (AGCM and ARCM)**

188 LMDZ4 (Hourdin et al., 2006; Li, 1999) is the atmospheric general circulation model developed and  
189 maintained by IPSL (Institut Pierre Simon Laplace). It has been widely used in previous phases of CMIP  
190 and PMIP projects. The resolution of the model is variable. Its global version used here (referred to as  
191 LMDZ4-global) is  $1.875^\circ$  in longitude and  $1.25^\circ$  in latitude with 19 layers in the vertical. It provides the  
192 boundary conditions to drive LMDZ4-regional. LMDZ4-regional (Li et al., 2012) is a regionally-  
193 oriented version of LMDZ4 with the same physics and same vertical discretisation, dedicated to the  
194 Mediterranean region. The zoomed-in model covers an effective domain of  $13^\circ\text{W}$  to  $43^\circ\text{E}$  and  $24^\circ\text{N}$  to  
195  $56^\circ\text{N}$  with a horizontal resolution of about 30 km inside the zoom. The rest of the globe outside this  
196 domain is considered to be the buffer-zone for LMDZ4-regional where a relaxation operation is  
197 performed to nudge the model with variables from the AGCM. The resolution of LMDZ4-regional  
198 decreases rapidly outside its effective domain. In both LMDZ4-global and LMDZ4-regional, land-  
199 surface processes, including the hydrological cycle, are taken into account through a full coupling with  
200 the surface model, ORCHIDEE.

### 201 **2.2 The regional oceanic model (ORCM)**

202 NEMOMED8 (Beuquier et al., 2010; Herrmann et al., 2010) is the regional Mediterranean configuration  
203 of the NEMO oceanic modelling platform (Madec, 2008). The horizontal domain includes the  
204 Mediterranean Sea and the nearby Atlantic Ocean which serves as a buffer zone (from  $11^\circ\text{W}$  to  $7.5^\circ\text{W}$ ).  
205 The horizontal resolution is  $1/8^\circ$  in longitude and  $1/8^\circ \cos\phi$  in latitude, i.e. 9km to 12km from the north  
206 to the south. The model has 43 layers of inhomogeneous thickness (from 7m at the surface to 200m in  
207 the depths) in the vertical. River discharges are accounted for as freshwater fluxes in the grids  
208 corresponding to the river mouths. A first dataset of river discharges represents 33 river mouths  
209 throughout the Mediterranean region. It contains monthly mean climatological values of runoff.



210 Interactive calculations of freshwater discharges from rivers by the land-surface model, ORCHIDEE,  
211 include 192 river mouths for the Mediterranean. The Black Sea, not included in NEMOMED8, counts  
212 as a river dumping freshwater into the Aegean. The deposit rate is calculated based on total runoff into  
213 the Black Sea, plus the net budget of precipitation (P) minus evaporation (E) over the Black Sea.

### 214 **2.3 Modelling Sequence**

215 As shown in Fig. 1, the first step in our modelling chain is to obtain SST and SIC values from an Earth  
216 System Model simulation able to reproduce global climate (for the past, present or future). We can  
217 reasonably hypothesise that major global climate information can transit from global SST and SIC. This  
218 hypothesis was deemed legitimate for climate downscaling purposes for Antarctic and Africa, in Krinner  
219 et al. (2014) and Hernández-Díaz et al. (2017) respectively. In the present work we use IPSL-CM5A  
220 (Dufresne et al., 2013) to extract relevant SST and SIC values to drive the AGCM (LMDZ4-global) and  
221 the ARCM (LMDZ4-regional). The next step is to run the two atmospheric models, LMDZ4-global and  
222 LMDZ4-regional, in the usual way as proposed by the AMIP community. This is the most expensive  
223 step, as atmospheric models are the most demanding in terms of computing resources. Fortunately, it is  
224 not necessary to run them for a long time as the atmosphere reaches equilibrium quickly. We applied  
225 30 years of simulation to both models. We consider this duration to be long enough to depict climate  
226 variability for the simulation of past events. The AGCM nudges the ARCM in the conventional way of  
227 one-way nesting for temperature, humidity, meridional and zonal wind every two hours. The nudging is  
228 done using an exponential relaxation procedure with a timescale of half an hour outside the zoom and  
229 10 days inside the zoom. Table S1 in the SOM summarises the forcings used, especially the orbital  
230 forcing and atmospheric CO<sub>2</sub>.

231 The necessary variables (surface air temperature, wind stress, P-E over the sea, heat fluxes) are provided  
232 by ARCM to NEMOMED8. The salinity and temperature conditions are provided in three dimensions  
233 in the buffer zone. River runoff depends on the configuration used. Table S2 in SOM details these  
234 boundary conditions.

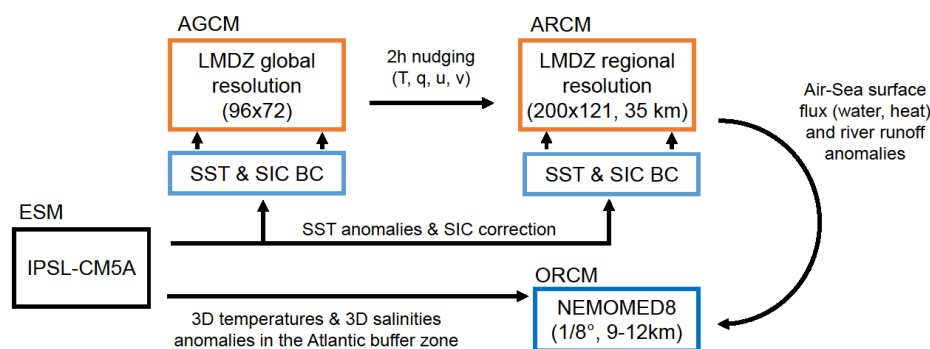
### 235 **2.4 Bias correction**

236 The sequential modelling chain, despite the lack of interactivity and feedback at interfaces, allows for  
237 error removal and bias correction at each step of the methodology. This adjustment is sometimes crucial,  
238 especially when model outputs need to be of very high quality to be incorporated into impact studies.  
239 This concept was further described in Krinner et al. (2019), as illustrated in Fig. 16 of their paper.  
240 Therefore, to enhance our confidence in the realism of the simulation results, bias-correction may be  
241 introduced when necessary. The correction method used in the present work generally follows the  
242 conventional procedure, which is based on the difference between the model outputs for present day  
243 simulations and actual observations. Biases corrected in this way, theoretically only valid for the



244 historical simulation (named HIST hereafter), are assumed to remain unchanged for past and future  
245 simulation scenarios. However, the transferability between past and future periods is questionable. There  
246 is no guarantee that the model error for a period is the same for other periods, even though the model  
247 physics may be the same. In addition, paleodata are often rare and incomplete, and so, are unsuitable for  
248 evaluation and correction of model errors. The most reliable basis is that established for the present day.  
249 The reader can find a full description of the bias corrections in the supplementary online material, “Text  
250 S2: Bias correction”.

251  
252



253  
254

255 **Figure 1: Flowchart of the modelling chain including the four main components: ESM, AGCM,**  
256 **ARCM and ORCM. BC: boundary condition, u: meridional wind, v: zonal wind, q: specific**  
257 **humidity, T: temperature, S: salinity, SST: sea surface temperature, SSS: sea surface salinities.**

### 258 3 Validation of the modelling chain for present-day climate 1970-1999

259 In this section, we evaluate the capacity of the model to reproduce the climate of the recent past, in  
260 particular, its ability to simulate sea surface characteristics as well as the Mixed Layer Depth (MLD)  
261 and oceanic convection patterns as these are key elements to reproduce the evolution of the  
262 Mediterranean Sea in past climate conditions.

#### 263 3.1 Experimental design

264 For the HIST experiment, we used SST and SIC observations (source: ERA-Interim) to force the  
265 AGCM. River runoff is from the climatology of Ludwig et al., (2009). Monthly mean climatological sea  
266 temperatures and salinities (from WOA) are used for the Atlantic boundary zone. HIST atmospheric  
267 simulations for both global and regional simulations have a duration of 30 years. The length of the HIST  
268 oceanic simulation is also 30 years, but obtained after a 150-year spin-up. The forcings for each



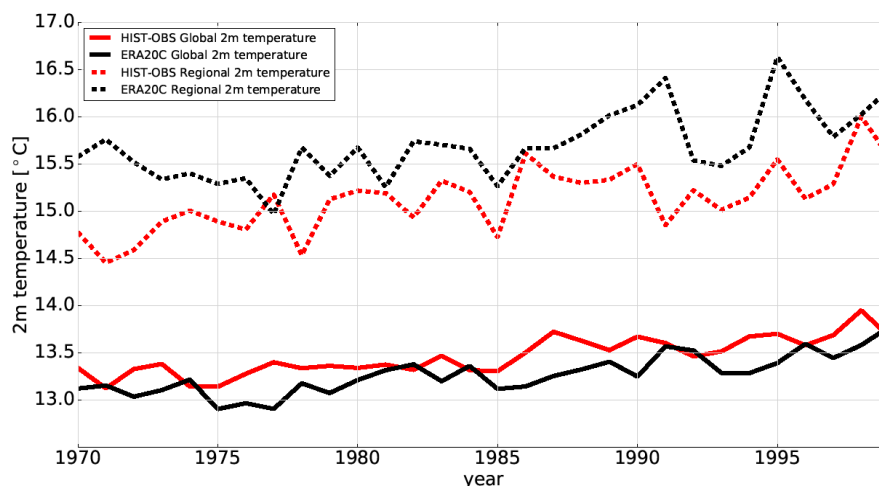


269 experiment are detailed in “Table S1” and Table S2” in the supplementary online material. Spin-up  
270 phases for each simulation are also shown from “Figure S4” to “Figure S7” for the overturning stream  
271 function and the index of stratification.

### 272 3.2 Evolution of temperatures

273 Figure 2 depicts the temporal evolution, between 1970 and 1999, of annual mean surface air  
274 temperatures at two metres in the atmospheric simulations (global and regional) compared to  
275 observations for the whole globe and over the Mediterranean region. The two models reproduce a range  
276 of temperatures similar to the observations, with the Mediterranean temperatures warmer than the global  
277 temperatures. The regional model reproduces the warming trend and aspects of the interannual  
278 variability which are quite close to observations.

279



280

281

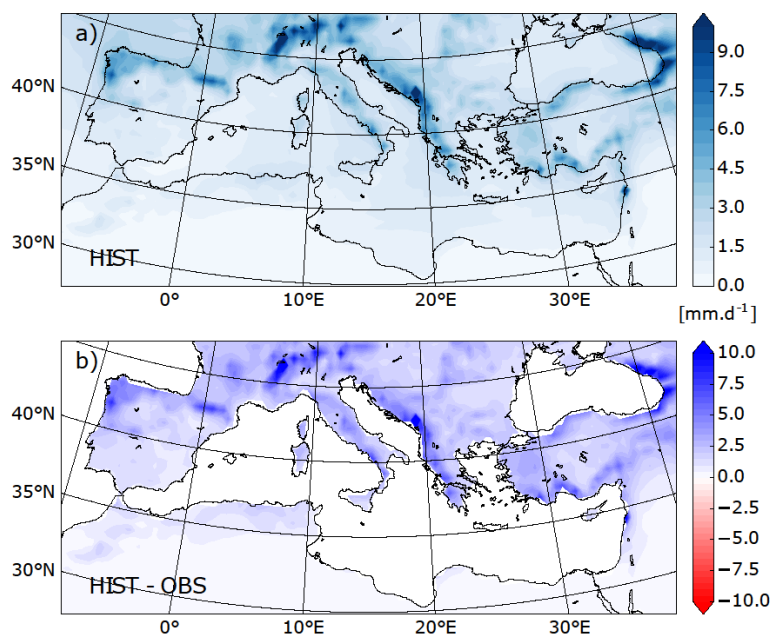
282 **Figure 2: Time series of annual mean surface air temperatures at 2 m in HIST (red) and ERA20C**  
283 **(black) for global average (solid lines) and Mediterranean-only average (dashed lines).**

### 284 3.3 Precipitation and freshwater budget

285 Figure 3 shows the average annual precipitation for 1970-1999 in HIST over the Mediterranean region  
286 and the differences with observations. The main features of the distribution of precipitation over the  
287 Mediterranean region are simulated, in particular the distinct contrast between the very low precipitation  
288 in the southern region and higher precipitation in the north. However, the regional model tends to  
289 overestimate precipitation over most of Europe, especially over the Alps, the Pyrenees, the Balkans and  
290 other mountainous regions. The freshwater budget over the Mediterranean Sea from observations and



291 the various simulations conducted in this study are summed up in table 3. (from a synthesis study by  
292 Sanchez-Gomez et al., 2011). The simulated continental precipitation is overestimated, but both the  
293 precipitation and evaporation over the Mediterranean Sea in HIST is very close to the observations.  
294  
295



296  
297 **Figure 3: Annual mean precipitation (mm/day) in HIST (panel a). Deviation of HIST simulation**  
298 **from observation-based CRU data (HIST-CRU, panel b, over land only, averaged over the entire**  
299 **simulation).**

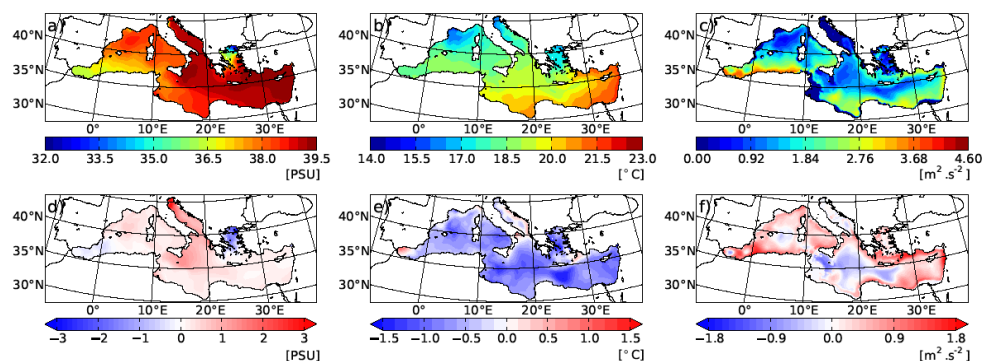
### 300 3.4 Mediterranean Sea surface characteristics

301 Figure 4 displays the temperatures and salinities of the Mediterranean Sea simulated in HIST and the  
302 deviations from observations. The model is able to capture the main characteristics of the pronounced  
303 west-east gradient of SSS in the Mediterranean Sea (Figure 4 a). Values are within the range of  
304 observations (mean bias = -0.32 PSU, error = 0.37 PSU, table 4). In the simulation, the Aegean Sea is  
305 not salty enough (about -1.5 PSU) and the Adriatic/Ionian Sea is too salty (+1 PSU).

306 The model reproduced the northwest to southeast temperature gradient, as shown in Figure 4b. However,  
307 the model shows a general cold bias (from -0.5 to -1.5 °C) over the entire Mediterranean (Figure 4e),  
308 due to the cold bias already observed for the air temperature at 2m in the regional atmospheric forcing  
309 (cf Figure 2).



310

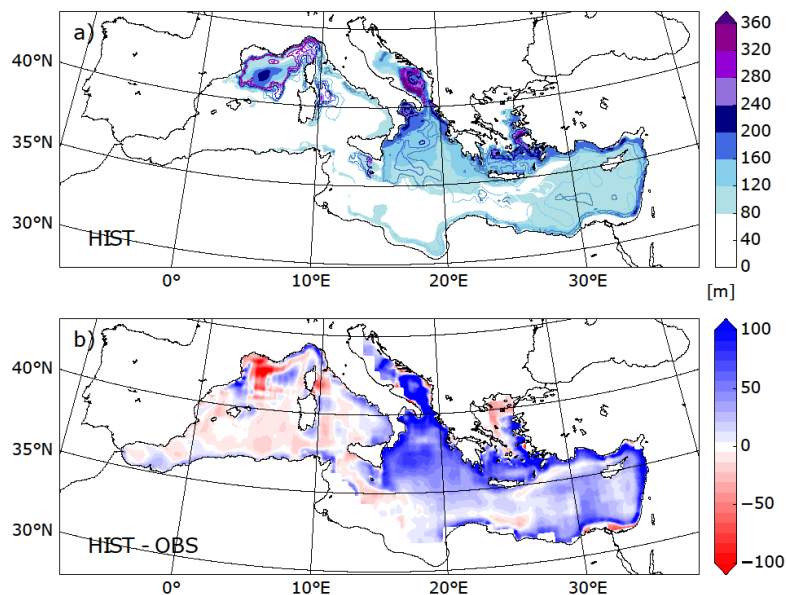


311

312

313 **Figure 4: Annual mean sea-surface salinity (left panels, SSS in PSU), sea-surface temperature**  
314 **(middle panels, SST in °C) and index of water column stratification (right panels, winter IS in**  
315 **m<sup>2</sup>/s<sup>2</sup>) simulated in HIST (top panels) and the HIST deviation from the observation-based**  
316 **MEDATLAS data (averaged over the entire simulation).**

317



318

319

320 **Figure 5: a) Mixed layer depth simulated in HIST (panel a, in m) and as deviation of HIST**  
321 **from observations of Houpert et al., (2015) averaged over the entire simulation.**



322

	SST	SSS	IS
Mean bias	0.64	-0.32	-0.91
RMS error	0.45	0.37	0.29

323

324 **Table 1: Mean bias of the HIST simulation expressed as the deviation from observations**  
325 **(MEDATLAS-II), and root mean square errors.**

### 326 3.4 Mediterranean Thermohaline circulation

327 Here, we evaluate the general characteristics of the simulated thermohaline circulation in regions where  
328 deep and intermediate water formation occurs. Figure 4c displays the stratification index (IS<sup>1</sup>) for HIST.  
329 IS is a vertical integration of the Brunt-Vaisala frequency. A lower IS implies that convection is more  
330 likely. The range of IS biases (Figure 4f), is from -1 to 1 m<sup>2</sup>.s<sup>-2</sup> (mean bias = -0.91 m<sup>2</sup>.s<sup>-2</sup>, error = 0.29  
331 m<sup>2</sup>.s<sup>-2</sup>). The model satisfactorily reproduces the convection in known intermediate and deep-water  
332 formation areas, namely the Gulf of Lions, the Adriatic Sea, the Ionian Sea, the Aegean Sea and the  
333 North Levantine.

334

335 Comparison with observations of the mixed-layer depth (Houpert et al., 2015) confirms that the model  
336 reproduces realistic intermediate and deep-water formation patterns (figure 5a), with a thicker MLD in  
337 the eastern basin and a shallower MLD in the Gulf of Lions (figure 5a).

338

339 We then analyse the simulated Mediterranean overturning circulation (figure 6). The Zonal Overturning  
340 stream Function (ZOF<sup>2</sup>) in figure 7a depicts the surface and intermediate circulation and the  
341 intermediate/deep circulation. The surface current from the Strait of Gibraltar flows up to 30°E and back  
342 to the Atlantic Ocean in the intermediate layers, through the Levantine Intermediate Water (LIW)

---

<sup>1</sup>  $IS(x, y, h) = \int_0^h N^2(x, y) z dz$ .  $N^2$  is the Brunt-Väisälä frequency. IS is calculated at each model grid  $(x, y)$  for a given depth  $h$  (set as the bottom of the sea, or as 1000 m when the depth is greater than 1000 m).

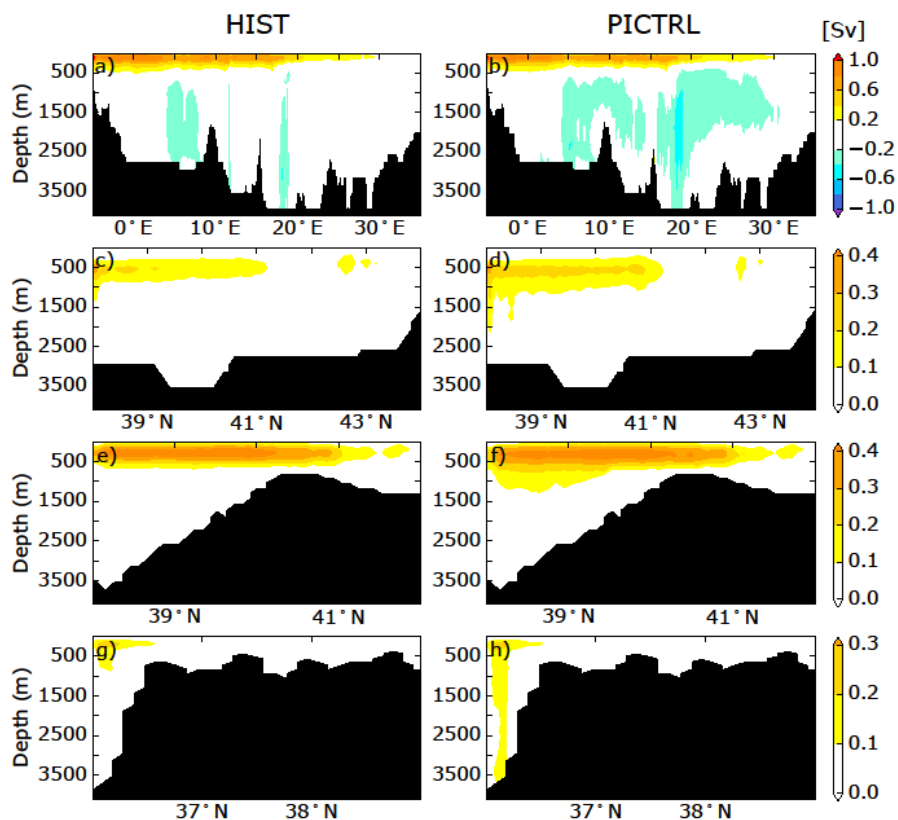
<sup>2</sup>  $ZOF(x, z) = \int_h^z \int_{y_s}^{y_n} u(x, y, z) dy dz$ .  $u$  is the zonal currents,  $h$  is the depth of the bottom,  $y_n$  and  $y_s$  are the north and south coordinates respectively.



343 outflow. Figure 6 c e and g represents the Meridional Overturning stream Function (MOF<sup>3</sup>) in the Gulf  
344 of Lions, the Adriatic Sea and the Aegean Sea, respectively. The surface cell in the longitude-depth plan  
345 is comparable to previous studies done with the same regional oceanic model, but with different forcings  
346 (Adloff et al., 2015; Somot et al., 2006): the mean strength of the surface cell ranges from 0.8 to 1.0 Sv,  
347 and the longitudinal extension is from 5°W to 30°E. The simulated intermediate and deep cells are  
348 recognized in existing studies as having different characteristics. Our simulated pattern is very close to  
349 a similar historical run in Adloff et al., (2015), but is weaker than a historical run in Somot et al., (2006)  
350 and a second historical configuration (with refined air-sea flux) in Adloff et al., (2015). A large spread  
351 between the models for this pattern indicates that there is still a lack of modelling capacity to simulate  
352 the deep circulation of the Mediterranean Sea.  
353

---

<sup>3</sup>  $MOF(y, z) = \int_h^z \int_{x_e}^{x_w} v(x, y, z) dx dz$ .  $v$  is the meridional currents,  $h$  is the depth of the bottom,  $x_w$  and  $x_e$  are the west and east coordinates respectively.



354

355 Figure 6: Zonal Overturning stream-Function (ZOF, first column from left, panels a, and b) integrated  
356 from north to south and shown as a longitude-depth section for the whole Mediterranean Sea, for HIST,  
357 and PICTRL simulations (from top to bottom), respectively. Other panels show Meridional Overturning  
358 stream-Function (MOF) shown as a latitude-depth section, integrated west/east for the Gulf of Lion  
359 (second column from left), the Adriatic/Ionian Sea (third column from left), and the Aegean Sea  
360 (averaged over the entire simulation for HIST and over the last 30 years of simulation for PICTRL).

### 361 3.5 Summary of Validation

362 Validation of our platform was based on the historical period, 1970 to 1999. The atmospheric simulation  
363 is consistent with observations for the air temperature at 2m at both global and regional scales. There is  
364 significant overestimation of precipitation over the land surrounding the Mediterranean Sea. However,  
365 the freshwater budget over the sea is close to observations for both evaporation and precipitation. When



366 freshwater river discharges into the Mediterranean Sea are bias-corrected against the observed  
367 climatology, the areas of intermediate and deep convection produced by the model are realistic. The  
368 thermohaline circulation is well captured by the oceanic model (compared to the simulations of Adloff  
369 et al., 2015 and Somot et al., 2006 for instance), which inspires confidence in our modelling platform  
370 for the investigations of past climate.

#### 371 **4 Application of the modelling chain to the Early Holocene**

372 In this section, we present results obtained when our sequential modelling chain is applied in a  
373 paleoclimate context, which was our initial motivation for developing this modelling tool. We chose to  
374 test the performance of our tool on the Early Holocene, a period marked by significant changes in climate  
375 and ocean dynamics over the Mediterranean basin, when the last sapropel event, S1, occurred in the  
376 Mediterranean Sea. Our experimental design relies on the comparison of two simulations: the Early  
377 Holocene (EHOL) with PICTRL based on pre-industrial conditions, the latter acting as a reference.

##### 378 **4.1 Experimental design**

379 As indicated in the general flowchart of our modelling platform, global SST and SIC are required to  
380 initiate our sequential modelling. The basic assumption is that the climate change signal can be  
381 reconstructed from global SST and SIC, an accepted practice within the climate modelling community.  
382 In this study, we use two existing long-term coupled simulations from IPSL-CM5A, one covering the  
383 pre-industrial period and the other covering the Early Holocene (around 9.5 ka). Taking the last 100  
384 years of each simulation, we construct a climatological SST and SIC. After conducting bias-correction,  
385 these outputs are then used to drive LMDZ-global and LMDZ-regional in a further step. The duration  
386 of the PICTRL and EHOL atmospheric simulations is 30 years (both global and regional models).  
387

388 Oceanic temperature and salinity in the Atlantic buffer-zone, as well as freshwater discharges from  
389 Mediterranean rivers, are all bias-corrected for NEMOMED8, as described in the general methodology.  
390 However, it needs to be pointed out that the reference point for the Nile river discharge is not modern  
391 observations but is set at pre-industrial values (2930 m<sup>3</sup>/s for annual mean, Vorosmarty, et al., 1998)  
392 corresponding to a period before construction of the Aswan dam. The oceanic simulation is 90 years for  
393 EHOL and 30 years for PICTRL, performed after a 200-year spin-up of PICTRL.

##### 394 **4.2 Climate features depicted in LMDZ-global**

395 Because Early Holocene simulations are mainly driven by insolation forcing, an important feature is the  
396 model response to seasonal temperatures. Figure 7 shows the difference between EHOL and PICTRL,  
397 as reproduced in LMDZ-global, for the summer/winter temperature, JJAS precipitation and JAS surface



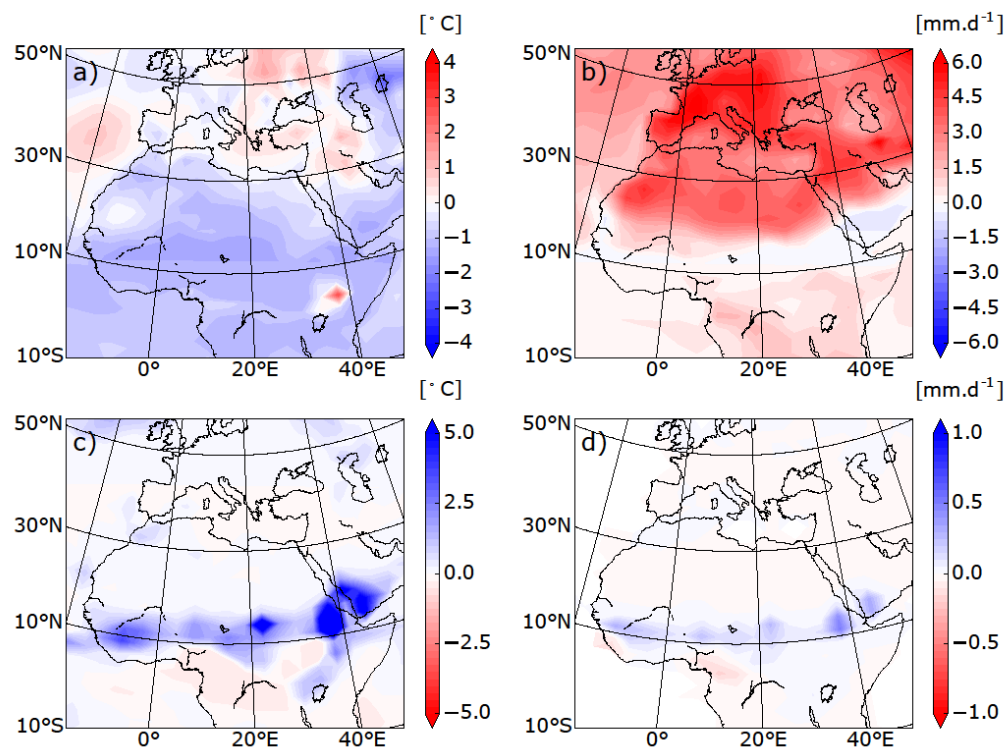
398 runoff. The atmospheric model imprints a stronger seasonality due to the increased Early Holocene  
399 insolation. Warmer summer temperatures over Europe and North Africa (+ 6 °C) and lower winter  
400 temperatures over Africa (-2 °C) reflect this feature. Variations of the precession also trigger an  
401 enhancement of the African Monsoon (+ 10 mm/day over the Ethiopian region). The main consequence  
402 of this increase in precipitation is an enhanced surface runoff over the Ethiopian region. This  
403 hydrological state is similar to the African Humid Period caused by the enhanced African Monsoon and  
404 the resultant increase in surface runoff, as shown in Rossignol-Strick et al. (1982).

405

406 Our results are similar to those of previous modelling exercises for the Early- and Mid-Holocene (e.g.  
407 Adloff et al., 2011; Bosmans et al., 2012; Braconnot et al., 2007; Marzin & Braconnot, 2009). They are  
408 also consistent with various reconstructions of Mid-Holocene precipitation (Harrison et al., 2014). A  
409 detailed comparison can be made with the Early Holocene simulation reported in Marzin and Braconnot  
410 (2009) which used the same orbital parameters and the same atmospheric model as we did. However,  
411 their model was coupled to an oceanic model, while we used an atmospheric model and prescribed SST  
412 and SIC as boundary conditions. Generally speaking, our results for both surface air temperature and  
413 precipitation are very similar to those of Marzin and Braconnot (2009), attesting to the validity of our  
414 approach using a simple atmospheric model constrained by boundary conditions. In the ensemble of  
415 PMIP simulations, available for the Early Holocene and mid-Holocene, there are some robust outputs  
416 for the climate response to orbital forcing but there are also some weaknesses common to most of the  
417 models (Braconnot et al., 2007; Kageyama et al., 2013). One of these weaknesses is the underestimation  
418 of the spread of the African monsoon towards North Africa. However, the increased discharge from the  
419 Nile river, induced by the enhanced monsoon is well supported by data (Adamson et al., 1980; Revel et  
420 al., 2014; Williams et al., 2000).

421





422

423 **Figure 7: Deviations between EHOL and PICTRL in LMDZ-GLOBAL for a) winter**  
424 **temperatures at 2m, b) summer temperatures a, c) June to September precipitation, and d) July**  
425 **to September surface runoff (averaged over the entire simulation).**

### 426 4.3 Mediterranean climate features with dynamical downscaling refinement

427 Figures 8, 9 and 10 show the results from the regional atmospheric model (LMDZ-regional, compared  
428 to those from LMDZ-global) for PICTRL and EHOL over the Mediterranean region. In both the global  
429 and regional simulations, an increased seasonality with warmer summers (+2 to +6 °C) and colder  
430 winters, especially over land (-3 to -1 °C, Figure 8), is depicted. Downscaling with LMDZ-regional  
431 slightly reduces the amplitude of the summer warming and shows a more homogenous signal in winter  
432 over land. The general circulation of the surface wind in PICTRL is west to east (Figure 9b), in line with  
433 the dominant winter regime of westerlies in the region. This important feature is almost missed in the  
434 global model (Figure 9a) which reproduces a lower intensity than the ARCM. In the regional model, the  
435 EHOL-PICTRL difference (figure 9d) shows a northward shift in position, with maximum changes  
436 occurring in the Levantine basin. The global model depicts a different response, with a dipole of change  
437 in wind intensity (figure 9c). The winter precipitation in EHOL, for ARCM (LMDZ-regional), increases  
438 over land in the Balkans and Italy and over the Adriatic, Ionian and Aegean Seas (figure 10b). These



439 changes are also present in the AGCM (LMDZ-global) that, furthermore, shows an increase in Spain  
440 and Portugal (figure 10a). It is in summer that the two models show the largest differences. In ARCM  
441 (LMDZ-regional), the Mediterranean basin experiences drier conditions, except in Italy and the North  
442 of the Balkans. Over the sea, precipitations slightly increase in EHOL (figure 10). However, the AGCM  
443 (LMDZ-global) shows drier conditions in the northern two thirds of the Mediterranean domain, with  
444 more humid conditions in the southern third (figure 10c). Changes in precipitation lead to unavoidable  
445 modifications in the runoff and river discharge into the Mediterranean Sea.

446

447 Although it is not straightforward to compare our “snapshot” simulations against environmental records  
448 (often used to reconstruct a timeline), our results compare well with the available data for this area (see  
449 supplementary online material, “Text S3: Comparison of model simulation outputs and reconstructed  
450 data for the Mediterranean basin”). Numerous proxies provide information on lake levels, paleo fires,  
451 pollen, isotopic signals recovered from speleothems which together describe the Mediterranean climate  
452 in the past. All of these proxies need to be brought together to provide a clear impression of the  
453 Mediterranean climate for this period (Magny et al., 2013; Peyron et al., 2011). Magny et al., (2007),  
454 based on records from Lake Acessa (Italy), suggested that aridification took place around 9200–7700  
455 cal BP. Zanchetta et al., (2007), based on data recovered from speleothems in Italy, conclude that the  
456 Western Mediterranean basin experienced enhanced rainfall during the S1 (10000-7000 cal BP). Jalut  
457 et al., (2009), using pollen data, suggest that the summers were short and dry and that there was abundant  
458 rainfall in winter (autumn and spring as well) and remarked that these wetter conditions favoured broad-  
459 leaf tree vegetation. Different proxies seem to provide contradictory information and therefore,  
460 seasonality must be introduced to reconcile them. Peyron et al., (2011) mentioned wet winters and dry  
461 summers during the ‘Holocene optimum’. Magny et al., (2013) support the hypothesis of seasonal  
462 contrast based on the analysis of multi-proxies.

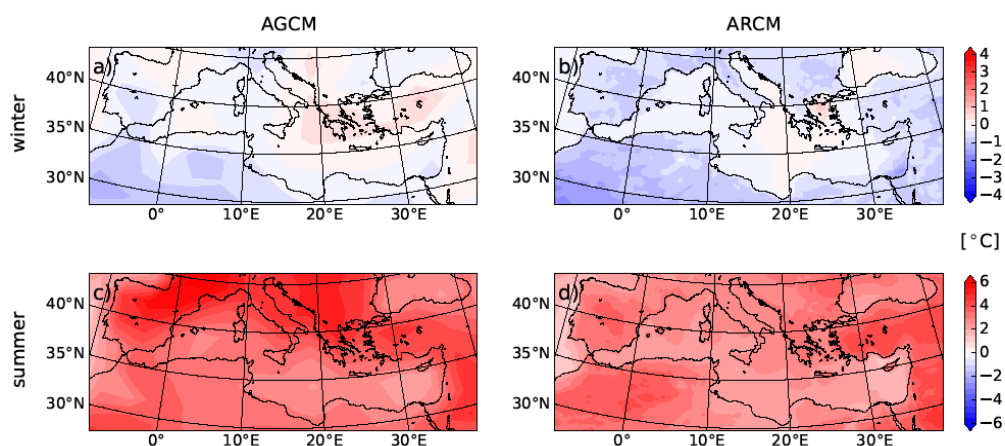
463

464 Our EHOL simulation successfully depicts this temperature contrast between winter and summer.  
465 Precipitation is enhanced in winter. In summer, the Mediterranean region is globally drier, except over  
466 Northern Italy and the northern Balkans. As explained above, there is no precipitation signal over  
467 Northern Africa, although evidence of paleo-lakes has been found in Algeria (Callot & Fontugne, 1992;  
468 Petit-Maire et al., 1991), Tunisia (Fontes & Gasse, 1991) and Libya (Gaven et al., 1981; Lezine &  
469 Casanova, 1991) during the early Holocene indicating increased rainfall in this area. In the  
470 supplementary material, we provide a comparison between simulated continental precipitation outputs  
471 and pollen reconstruction data. This comparison shows that the winter precipitation anomalies are  
472 consistent in both cases but that there is a distinct difference in summer values due to the more contrasted  
473 summer in the EHOL simulation (supplementary material 1).

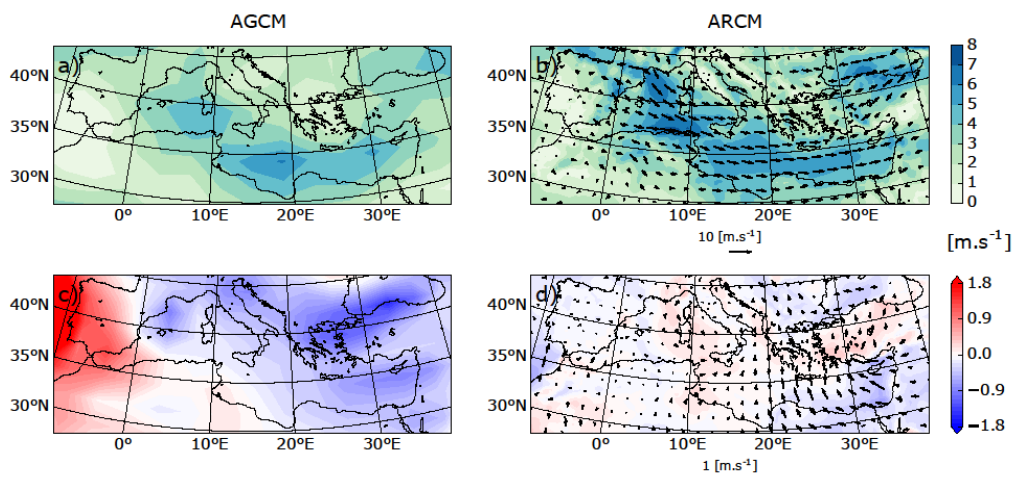
474



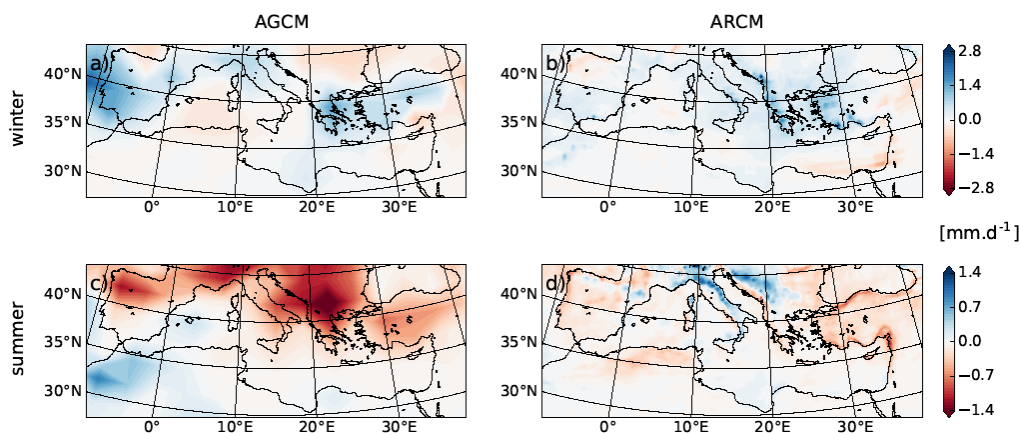
475 Peyron et al., (2017) simulated precipitation changes over the Mediterranean region for Mid and Late  
 476 Holocene using an atmospheric regional model. Their simulations and those presented in this study are  
 477 quite difficult to compare because of the period simulated (mid and late Holocene/ Early Holocene) and  
 478 the reference period used to compare them (Present-day/Pre-industrial).  
 479  
 480



481  
 482 **Figure 8: Deviations between EHOL and PICTRL for winter temperatures at 2m (first row) and**  
 483 **in summer temperature at 2m (second row), for the AGCM (first column) and the ARCM (second**  
 484 **column), averaged over the entire simulation.**



485  
 486 **Figure 9: Winter wind-speed in PICTRL (first row) for a) the AGCM and b) the ARCM.**  
 487 **Deviations (EHOL-PICTRL, second row) for c) the AGCM and d) the ARCM, averaged over the**  
 488 **entire simulation.**



489

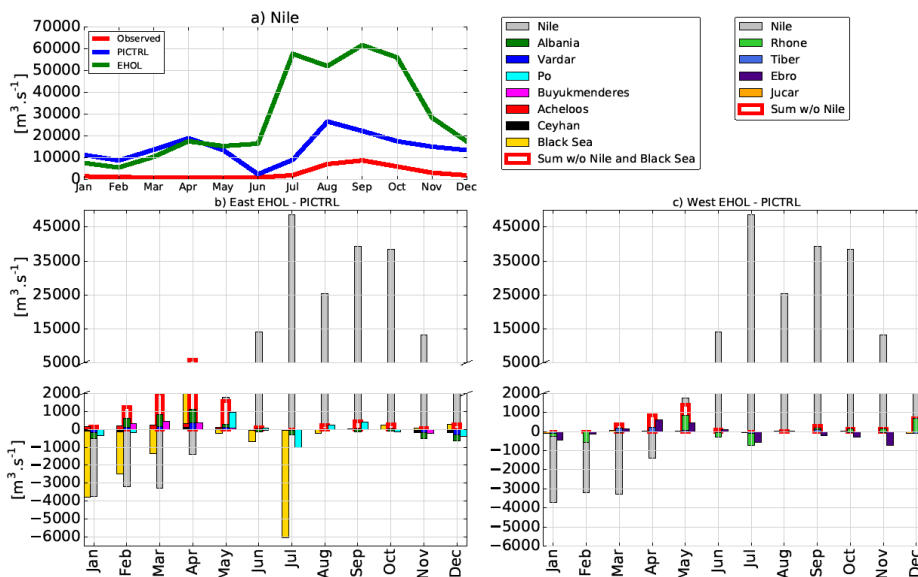
490 **Figure 10: Deviations between EHOL and PICTRL for winter precipitation (first row) and in**  
491 **summer precipitation (second row), for AGCM (first column) and ARCM (second column),**  
492 **averaged over the entire simulation.**

#### 493 4.4 Hydrological changes

494 Figure 11 shows the runoff simulated by the atmospheric model. The Nile River is shown in Figure 11a.  
495 Figures 11b and 11c plot the anomalies in river discharge between EHOL and PICTRL. The signal for  
496 the simulated Nile runoff in PICTRL shows an increase due to an overestimation of precipitation  
497 compared to pre-damming values. Both observations and simulations reach their maxima in summer.  
498

499 Figure 11 b and c show that the anomaly in freshwater supply into the Eastern Mediterranean basin in  
500 summer and autumn is mainly due to the Nile River. However, in winter, the Albanian rivers (Drini,  
501 Mat, Dures, Shkumbin and Vjosa) as well as the Vardar and the Buyukmenderes, produce positive  
502 anomalies in EHOL, due to enhanced winter continental precipitation in this simulation (figure 10 b and  
503 e). In EHOL, the supplementary winter freshwater input is less pronounced for the western basin than  
504 for the eastern basin. However, the North African rivers have not been represented because precipitation  
505 has not changed much in their catchment area (figure 10 b and e).

506



507  
 508 **Figure 11: a) climatological runoff of the Nile River: observed pre-damming values (red), PICTRL**  
 509 **(blue), EHOL (green), EHOL – PICTRL anomalies applied to observations. Absolute monthly**  
 510 **anomalies between EHOL and PICTRL in the simulated river runoff for b) rivers flowing into**  
 511 **the eastern basin, c) rivers flowing into the western basin including the Nile River (the scale is**  
 512 **different between the upper and lower b) and c) sub figures).**  
 513

Experiments/variables (mm/yr)	Evaporation	Precipitation	River runoff
OBS	1129	426	102-142
HIST	1106	443	74
PICTRL	1031	451	98
EHOL	1094	460	225

514 Table 2: The Mediterranean Sea freshwater budget. OBS is a summary of Sanchez-Gomez et al, 2011  
 515 (for the period 1958-2008). River discharges in HIST are taken from the climatology of Ludwig et al.,  
 516 2009. The same applies to PICTRL with the Nile set at its pre-industrial (pre-damming) value, 2930  
 517 m<sup>3</sup>/s, annually (Rivdis). River discharges in EHOL are based on changes in continental runoff between  
 518 EHOL and PICTRL.  
 519



520 **4.5 Changes in water properties of the Mediterranean Sea**

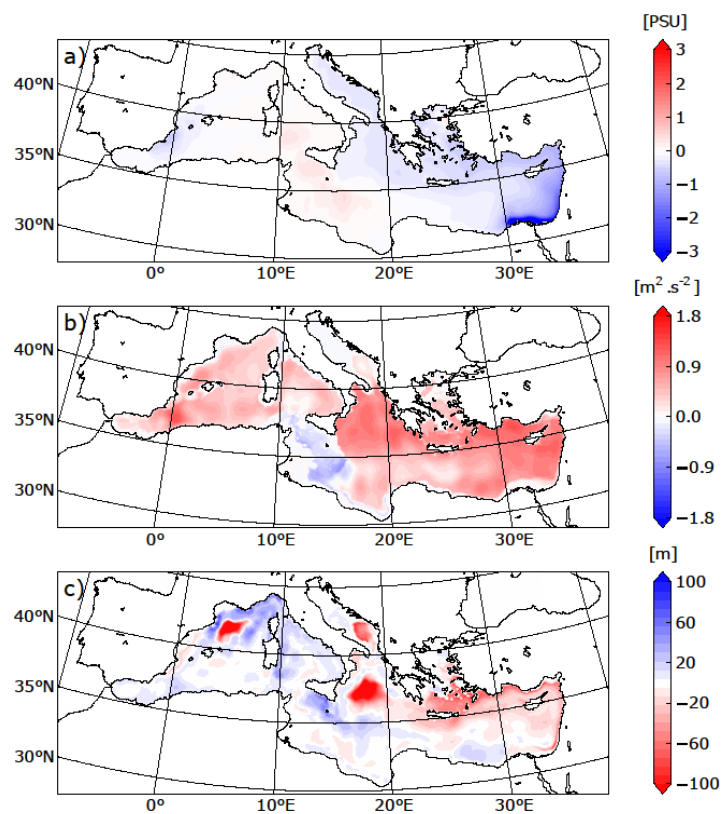
521 At the end of our modelling chain, we can examine changes in the properties of the Mediterranean  
522 seawater produced by NEMOMED8 for PICTRL and EHOL. It is important to mention at this stage,  
523 that for the correction of the river runoff the reference is the pre-industrial state, and not the historical  
524 simulation (as is the case for SST and SIC). Our aim was to keep river runoff anomalies free of  
525 anthropogenic influence. In addition, the fact that the “pre-industrial” Nile river runoff (in other words  
526 before damming) is well known influenced this choice. Figure 12 shows changes (EHOL minus PICTR)  
527 for sea surface salinities, stratification index and MLD. The freshwater inputs from the Nile and the  
528 north-eastern margin imply a lower salinity in the eastern basin. This decrease in salinity enhances  
529 stratification throughout the Mediterranean Sea (with the exception of the Sicily Sea) and affects the  
530 convection areas by decreasing the MLD. This global stratification in EHOL is followed by a general  
531 reduction in the thermohaline circulation compared to PICTRL (ZOF and MOF, figure 13 a, b, c, d).

532

533 Numerous studies have documented the sapropel event, S1 and the state of the Mediterranean Sea that  
534 caused it. Emeis et al., (2000), mentioned a decreased SSS during this period in both the eastern and  
535 western basins (As did Kallel et al., (1997) in the Tyrrhenian basin). In the subsection “*Sea Surface*  
536 *Temperatures*” and “*Sea Surface Salinity*” of the section “Text S3” in the supplementary online material,  
537 we compared the simulated SST and SSS to reconstructions. Although simulated SST is in good  
538 agreement with the reconstructed data, there is a gap between the simulated SSS and reconstructions.  
539 This discrepancy is not surprising. Indeed, there are many explanations for the underestimation in our  
540 model of the salinity. One of them is a common weakness in Early to Mid-Holocene simulations,  
541 namely, the underestimation of the northward spread of the African monsoon and therefore, the  
542 underestimation of the freshwater flow from North Africa. Adloff (2011), already pointed to a shortfall  
543 in freshwater input to reconcile the simulated and observed SSS during the Early Holocene. Our oceanic  
544 simulation depicts these behaviours well and is similar to previous modelling studies with lower  
545 resolution (Adloff et al., 2011; Bosmans et al., 2015; Myers et al., 1998).

546

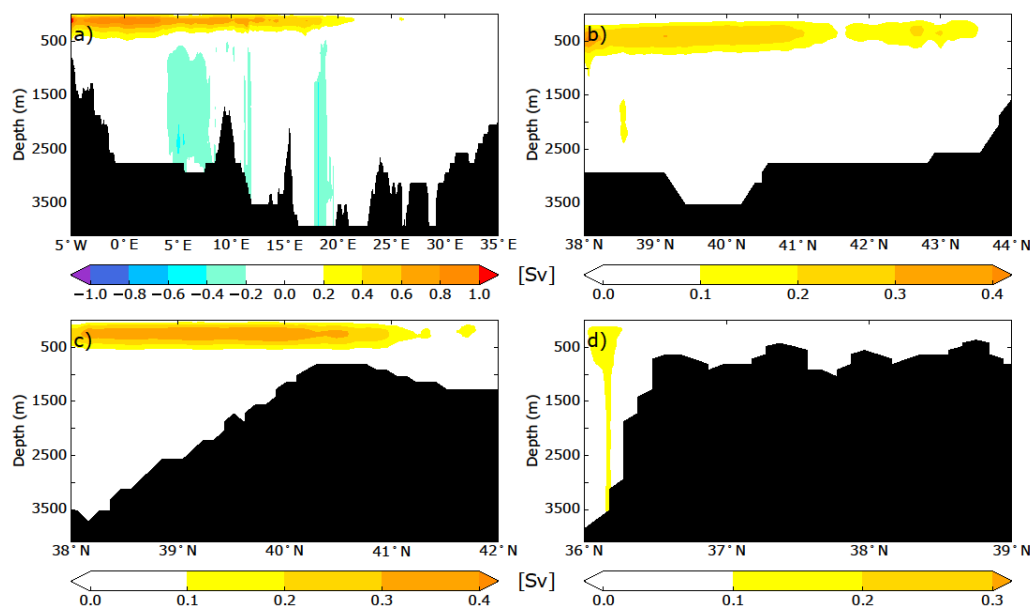
547



548

549 **Figure 12: Deviations between EHOL and PICTRL in a) sea surface salinity, b) stratification**

550 **index, c) mixed-layer depth, averaged over the last 30 years of simulation**



551

552 **Figure 13: ZOF (a) and MOF (b, Gulf of Lion, c, Adriatic/Ionian Sea, d, Ionian Sea) for EHOL**  
553 **experiment, averaged over the last 30 years of simulation.**

## 554 **5 Conclusion and perspectives for the modelling platform**

555

556 This study aimed to develop a modelling platform to simulate different climatic conditions of the  
557 Mediterranean basin. We developed a useful regional climate investigation platform with high spatial  
558 resolution over the Mediterranean region. This is particularly relevant for the study of impacts on the  
559 circulation of the Mediterranean Sea. The model chain has been evaluated for the historical period. We  
560 have presented Early Holocene simulations as an example of the potential of this platform to simulate  
561 past climate. For the Early Holocene, our model reproduced satisfactorily the global and regional climate  
562 features, compared to the observed data. Our platform allowed, for the first time, the generation of a  
563 high-resolution freshwater budget for this period, with a particular focus on continental precipitation, a  
564 key factor for the Mediterranean Sea in the assessment of its impact on circulation during the onset of  
565 the sapropel event, S1. An important limitation of our sequential approach is the fact that it does not  
566 take account of feedback of ocean changes on atmospheric circulation. However, this architecture allows  
567 bias correction, conducted at different levels of the platform. One way to overcome this problem would  
568 be to consider an “asynchronous mode”, namely, to take account of feedback from the ocean component  
569 to the atmosphere at a yearly or decadal frequency.

570





571 Two other issues need to be discussed for the Early Holocene. The first one is sea level, which was 20  
572 metres lower than the present day (Peltier et al., 2015). For the sake of simplicity, we did not take into  
573 account this difference of sea level in the EHOL simulation. The second issue is the timing of the  
574 (re)connection between the Black Sea and the Aegean Sea. This topic is still being debated. Sperling et  
575 al., (2003) suggested this reconnection occurred around 8.4 ka BP, while by the calculations of Soulet  
576 et al., (2011) it happened around 9 ka BP. Other studies found that an overflow from the Black Sea likely  
577 occurred before this reconnection due to Fennoscandian ice-sheet melting during the deglaciation  
578 (Chepalyga, 2007; Majoret al., 2002; Soulet et al., 2011). For the purposes of this work, we decided to  
579 maintain the Bosphorus open in our simulation, with the water exchange set at its modern value.

580

581 The modelling sequence, moving from global simulation at low resolution to high-resolution regional  
582 ocean modelling, avoids the problem of boundary conditions, and provides a fully consistent platform  
583 that may be used for many paleoclimate studies. We focused here on the Early Holocene period but this  
584 architecture could be used to study other periods investigated in MIPs, such as the Last Glacial  
585 Maximum or the deposition of older sapropels, from the Pliocene to the Quaternary, as long as the  
586 tectonics remain mainly unchanged (PMIP, PlioMIP).

587

588

589 **Code and data availability.** The current version of LMDZ and NEMO are available from the project website:  
590 [https://forge.ipsl.jussieu.fr/igcmg\\_doc/wiki/DocImodelBImdz](https://forge.ipsl.jussieu.fr/igcmg_doc/wiki/DocImodelBImdz) and <http://forge.ipsl.jussieu.fr/nemo/wiki/Users>  
591 under the terms of the CeCill license for LMDZ and NEMO both. The exact version of the model used to produce  
592 the results used in this paper is archived on Zenodo (Vadsaria et al., 2019), as are input data and scripts to run the  
593 model and produce the plots for all the simulations presented in this paper.

594

595 **Author's contribution.** This study was co-designed and approved by all co-authors. The simulation  
596 protocol was constructed by TV and LL from a modelling architecture provided by LL. TV conducted  
597 the numerical simulations and drafted the first version of the manuscript. All co-authors are largely  
598 involved in the writing and revision of the manuscript.

599

600 **Acknowledgments.** We thank Mary Minnock for her professional English revision. This work was  
601 supported by the French National program LEFE "HoMoSapiENS". This work was granted access to  
602 the HPC resources of TGCC under the allocation 2017-A0010102212, 2018-A0030102212 and 2018-  
603 A004-01-00239 made by GENCI.

604

605

606



607 **References**

- 608 Adloff, F., Mikolajewicz, U., Kučera, M., Grimm, R., Maier-Reimer, E., Schmiedl, G. and Emeis, K.  
609 C.: Upper ocean climate of the Eastern Mediterranean Sea during the Holocene Insolation Maximum -  
610 A model study, *Clim. Past*, 7(4), 1103–1122, doi:10.5194/cp-7-1103-2011, 2011.
- 611 Adloff, F., Somot, S., Sevault, F., Jordà, G., Aznar, R., Déqué, M., Herrmann, M., Marcos, M., Dubois,  
612 C., Padorno, E., Alvarez-Fanjul, E. and Gomis, D.: Mediterranean Sea response to climate change in an  
613 ensemble of twenty first century scenarios, *Clim. Dyn.*, 45(9–10), 2775–2802, doi:10.1007/s00382-015-  
614 2507-3, 2015.
- 615 Artale, V.: Role of surface fluxes in ocean general circulation models using satellite sea surface  
616 temperature: Validation of and sensitivity to the forcing frequency of the Mediterranean thermohaline  
617 circulation, *J. Geophys. Res.*, 107(C8), 3120, doi:10.1029/2000JC000452, 2002.
- 618 Artale, V., Calmanti, S., Carillo, A., Dell’Aquila, A., Herrmann, M., Pisacane, G., Ruti, P. M., Sannino,  
619 G., Struglia, M. V., Giorgi, F., Bi, X., Pal, J. S. and Rauscher, S.: An atmosphere–ocean regional climate  
620 model for the Mediterranean area: Assessment of a present climate simulation, *Clim. Dyn.*, 35(5), 721–  
621 740, doi:10.1007/s00382-009-0691-8, 2010.
- 622 Béranger, K., Drillet, Y., Houssais, M.-N., Testor, P., Bourdallé-Badie, R., Alhammoud, B., Bozec, A.,  
623 Mortier, L., Bouruet-Aubertot, P. and Crépon, M.: Impact of the spatial distribution of the atmospheric  
624 forcing on water mass formation in the Mediterranean Sea, *J. Geophys. Res.*, 115(C12), C12041,  
625 doi:10.1029/2009JC005648, 2010.
- 626 Beuvier, J., Sevault, F., Herrmann, M., Kontoyiannis, H., Ludwig, W., Rixen, M., Stanev, E., Branger,  
627 K. and Somot, S.: Modeling the Mediterranean Sea interannual variability during 1961–2000: Focus on  
628 the Eastern Mediterranean Transient, *J. Geophys. Res. Ocean.*, 115(8), 1–27,  
629 doi:10.1029/2009JC005950, 2010.
- 630 Chen, J., Brissette, F. P. and Leconte, R.: Uncertainty of downscaling method in quantifying the impact  
631 of climate change on hydrology, *J. Hydrol.*, 401(3–4), 190–202, doi:10.1016/j.jhydrol.2011.02.020,  
632 2011.
- 633 Chepalyga, A. L.: The late glacial great flood in the Ponto-Caspian basin, in *The Black Sea Flood*  
634 *Question: Changes in Coastline, Climate, and Human Settlement*, pp. 119–148., 2007.
- 635 Dell’Aquila, A., Calmanti, S., Ruti, P., Struglia, M. V., Pisacane, G., Carillo, A. and Sannino, G.: Effects  
636 of seasonal cycle fluctuations in an A1B scenario over the Euro-Mediterranean region, *Clim. Res.*, 52(1),  
637 135–157, doi:10.3354/cr01037, 2012.
- 638 Drobinski, P., Anav, A., Lebeaupin Brossier, C., Samson, G., Stéfanon, M., Bastin, S., Baklouti, M.,  
639 Béranger, K., Beuvier, J., Bourdallé-Badie, R., Coquart, L., D’Andrea, F., de Noblet-Ducoudré, N.,



- 640 Diaz, F., Dutay, J. C., Ethé, C., Foujols, M. A., Khvorostyanov, D., Madec, G., Mancip, M., Masson,  
641 S., Menut, L., Palmieri, J., Polcher, J., Turquety, S., Valcke, S. and Viovy, N.: Model of the Regional  
642 Coupled Earth system (MORCE): Application to process and climate studies in vulnerable regions,  
643 *Environ. Model. Softw.*, 35, 1–18, doi:10.1016/j.envsoft.2012.01.017, 2012.
- 644 Dufresne, J. L., Foujols, M. A., Denvil, S., Caubel, A., Marti, O., Aumont, O., Balkanski, Y., Bekki, S.,  
645 Bellenger, H., Benshila, R., Bony, S., Bopp, L., Braconnot, P., Brockmann, P., Cadule, P., Cheruy, F.,  
646 Codron, F., Cozic, A., Cugnet, D., de Noblet, N., Duvel, J. P., Ethé, C., Fairhead, L., Fichefet, T.,  
647 Flavoni, S., Friedlingstein, P., Grandpeix, J. Y., Guez, L., Guilyardi, E., Hauglustaine, D., Hourdin, F.,  
648 Idelkadi, A., Ghattas, J., Joussaume, S., Kageyama, M., Krinner, G., Labetoulle, S., Lahellec, A.,  
649 Lefebvre, M. P., Lefevre, F., Levy, C., Li, Z. X., Lloyd, J., Lott, F., Madec, G., Mancip, M., Marchand,  
650 M., Masson, S., Meurdesoif, Y., Mignot, J., Musat, I., Parouty, S., Polcher, J., Rio, C., Schulz, M.,  
651 Swingedouw, D., Szopa, S., Talandier, C., Terray, P., Viovy, N. and Vuichard, N.: Climate change  
652 projections using the IPSL-CM5 Earth System Model: From CMIP3 to CMIP5, *Clim. Dyn.*, 40(9–10),  
653 2123–2165, doi:10.1007/s00382-012-1636-1, 2013.
- 654 Giorgi, F.: Climate change hot-spots, *Geophys. Res. Lett.*, 33(8), 1–4, doi:10.1029/2006GL025734,  
655 2006.
- 656 Goubanova, K. and Li, L.: Extremes in temperature and precipitation around the Mediterranean basin  
657 in an ensemble of future climate scenario simulations, *Glob. Planet. Change*, 57(1), 27–42,  
658 doi:https://doi.org/10.1016/j.gloplacha.2006.11.012, 2007.
- 659 Herrmann, M., Sevault, F., Beuvier, J. and Somot, S.: What induced the exceptional 2005 convection  
660 event in the northwestern Mediterranean basin? Answers from a modeling study, *J. Geophys. Res.*  
661 *Ocean.*, 115(12), 1–19, doi:10.1029/2010JC006162, 2010.
- 662 Houpert, L., Testor, P., de Madron, X. D., Somot, S., D’Ortenzio, F., Estournel, C. and Lavigne, H.:  
663 Seasonal cycle of the mixed layer, the seasonal thermocline and the upper-ocean heat storage rate in the  
664 Mediterranean Sea derived from observations, *Prog. Oceanogr.*, 132, 333–352,  
665 doi:10.1016/j.pocean.2014.11.004, 2015.
- 666 Hourdin, F., Musat, I., Bony, S., Braconnot, P., Codron, F., Dufresne, J. L., Fairhead, L., Filiberti, M.  
667 A., Friedlingstein, P., Grandpeix, J. Y., Krinner, G., LeVan, P., Li, Z. X. and Lott, F.: The LMDZ4  
668 general circulation model: Climate performance and sensitivity to parametrized physics with emphasis  
669 on tropical convection, *Clim. Dyn.*, 27(7–8), 787–813, doi:10.1007/s00382-006-0158-0, 2006.
- 670 Jost, A., Lunt, D., Abe-Ouchi, A., Abe-Ouchi, A., Peyron, O., Valdes, P. J. and Ramstein, G.: High-  
671 resolution simulations of the last glacial maximum climate over Europe: A solution to discrepancies  
672 with continental palaeoclimatic reconstructions?, *Clim. Dyn.*, 24(6), 577–590, doi:10.1007/s00382-005-  
673 0009-4, 2005.



- 674 Krinner, G., Llargeron, C., Ménégoz, M., Agosta, C. and Brutel-Vuilmet, C.: Oceanic forcing of  
675 Antarctic climate change: A study using a stretched-grid atmospheric general circulation model, *J.*  
676 *Clim.*, 27(15), 5786–5800, doi:10.1175/JCLI-D-13-00367.1, 2014.
- 677 De Lange, G. J., Thomson, J., Reitz, A., Slomp, C. P., Speranza Principato, M., Erba, E. and Corselli,  
678 C.: Synchronous basin-wide formation and redox-controlled preservation of a Mediterranean sapropel,  
679 *Nat. Geosci.*, 1(9), 606–610, doi:10.1038/ngeo283, 2008.
- 680 Lebeaupin Brossier, C., Béranger, K., Deltel, C. and Drobinski, P.: The Mediterranean response to  
681 different space-time resolution atmospheric forcings using perpetual mode sensitivity simulations,  
682 *Ocean Model.*, 36(1–2), 1–25, doi:10.1016/j.ocemod.2010.10.008, 2011.
- 683 Li, L., Casado, A., Congedi, L., Dell’Aquila, A., Dubois, C., Alizade, A., L’Heveder, B., Lionello, P.,  
684 Sevault, F., Somot, S., Ruti, P. and Zampieri, M.: Modeling of the Mediterranean climate system, in  
685 *MedCLIVAR book II: Mediterranean climate system, developments in earth environmental sciences.*  
686 Elsevier, Amsterdam, edited by P. Lionello, P. Boscolo, and R. Boscolo, Elsevier, Amsterdam., 2012.
- 687 Li, Z. X.: Ensemble atmospheric GCM simulation of climate interannual variability from 1979 to 1994,  
688 *J. Clim.*, 12(4), 986–1001, doi:10.1175/1520-0442(1999)012<0986:EAGSOC>2.0.CO;2, 1999.
- 689 Ludwig, P., Shao, Y., Kehl, M. and Weniger, G. C.: The Last Glacial Maximum and Heinrich event I  
690 on the Iberian Peninsula: A regional climate modelling study for understanding human settlement  
691 patterns, *Glob. Planet. Change*, 170(January), 34–47, doi:10.1016/j.gloplacha.2018.08.006, 2018.
- 692 Ludwig, W., Dumont, E., Meybeck, M. and Heussner, S.: River discharges of water and nutrients to the  
693 Mediterranean and Black Sea: Major drivers for ecosystem changes during past and future decades?,  
694 *Prog. Oceanogr.*, 80(3–4), 199–217, doi:10.1016/j.pocean.2009.02.001, 2009.
- 695 Macias, D. M., Garcia-Gorriz, E. and Stips, A.: Productivity changes in the Mediterranean Sea for the  
696 twenty-first century in response to changes in the regional atmospheric forcing, *Front. Mar. Sci.*,  
697 2(660841), doi:10.3389/fmars.2015.00079, 2015.
- 698 Madec, G.: NEMO ocean engine, Note du Pôle de modélisation, Institut Pierre-Simon Laplace (IPSL),  
699 France, No 27, ISSN No 1288-1619., 2008.
- 700 Major, C., Ryan, W., Lericolais, G. and Hajdas, I.: Constraints on Black Sea outflow to the Sea of  
701 Marmara during the last glacial-interglacial transition, *Mar. Geol.*, 190, 19–34, 2002.
- 702 Mikolajewicz, U.: Modeling mediterranean ocean climate of the last glacial maximum, *Clim. Past*, 7(1),  
703 161–180, doi:10.5194/cp-7-161-2011, 2011.
- 704 Millot, C. and Taupier-Letage, I.: *Circulation in the Mediterranean Sea*, pp. 29–66, Springer, Berlin,  
705 Heidelberg., 2005.



- 706 Peltier, W. R., Argus, D. F. and Drummond, R.: Space geodesy constrains ice age terminal deglaciation:  
707 The global ICE-6G\_C (VM5a) model, *J. Geophys. Res. Solid Earth*, 2015(120), 450–487,  
708 doi:10.1002/2014JB011176.Received, 2015.
- 709 Ramstein, G., Kageyama, M., Guiot, J., Wu, H., Hély, C., Krinner, G. and Brewer, S.: How cold was  
710 Europe at the Last Glacial Maximum? A synthesis of the progress achieved since the first PMIP model-  
711 data comparison, *Clim. Past*, 3(2), 331–339, doi:10.5194/cp-3-331-2007, 2007.
- 712 Sanchez-Gomez, E., Somot, S., Josey, S. A., Dubois, C., Elguindi, N. and Déqué, M.: Evaluation of  
713 Mediterranean Sea water and heat budgets simulated by an ensemble of high resolution regional climate  
714 models, *Clim. Dyn.*, 37(9–10), 2067–2086, doi:10.1007/s00382-011-1012-6, 2011.
- 715 Sevault, F., Somot, S., Alias, A., Dubois, C., Lebeaupin-Brossier, C., Nabat, P., Adolff, F., Deque, M.  
716 and Decharme, B.: A fully coupled Mediterranean regional climate system model: design and evaluation  
717 of the ocean component for the 1980 2012 period, *Tellus A*, 1, 1–32, 2014.
- 718 Somot, S., Sevault, F. and Déqué, M.: Transient climate change scenario simulation of the  
719 Mediterranean Sea for the twenty-first century using a high-resolution ocean circulation model, *Clim.*  
720 *Dyn.*, 27(7–8), 851–879, doi:10.1007/s00382-006-0167-z, 2006.
- 721 Somot, S., Sevault, F., Déqué, M. and Crépon, M.: 21st century climate change scenario for the  
722 Mediterranean using a coupled atmosphere–ocean regional climate model, *Glob. Planet. Chang.*, 63(2–  
723 3), 112–126, doi:10.1016/j.gloplacha.2007.10.003, 2008.
- 724 Soulet, G., Ménot, G., Garreta, V., Rostek, F., Zaragosi, S., Lericolais, G. and Bard, E.: Black Sea  
725 “Lake” reservoir age evolution since the Last Glacial — Hydrologic and climatic implications, *Earth*  
726 *Planet. Sci. Lett.*, 308(1–2), 245–258, doi:10.1016/j.epsl.2011.06.002, 2011.
- 727 Sperling, M., Schmiedl, G., Hemleben, C., Emeis, K. C., Erlenkeuser, H. and Grootes, P. M.: Black Sea  
728 impact on the formation of eastern Mediterranean sapropel S1? Evidence from the Marmara Sea,  
729 *Palaeogeogr. Palaeoclimatol. Palaeoecol.*, 190, 9–21, doi:10.1016/S0031-0182(02)00596-5, 2003.
- 730 Swingedouw, D., Colin, C., Eynaud, F. and Ayache, M.: Impact of freshwater release in the  
731 Mediterranean Sea on the North Atlantic climate, *Clim. Dyn. Submitt.*, 2018.
- 732 Vadsaria, T., Li, L., Ramstein, G., & Dutay, J.-C.: Model and output for Vadsaria et al, “Development  
733 of a sequential tool LMDZ-NEMO-med-V1 for global to regional past climate simulation over the  
734 Mediterranean basin: an early Holocene case study”, GMD publication, doi:[10.5281/zenodo.3258409](https://doi.org/10.5281/zenodo.3258409),  
735 2019.
- 736 Vorosmarty, C. J., Feteke, B. M. and Tucker, B. A.: *Global River Discharge, 1807-1991*, V. 1.1  
737 (RivDIS), 1998.



738 de Zolt, S., Lionello, P. and Malguzzi, P.: Implementation of an aorc in the mediterranean sea, 2003.

739

740

741